A variationally calculated room temperature line-list for H_2O_2

Ahmed F. Al-Refaie

Department of Physics and Astronomy, University College London, London, WC1E 6BT, UK

Roman I. Ovsyannikov

Institute of Applied Physics, Russian Academy of Sciences, Ulyanov Street 46, Nizhny Novgorod, Russia 603950

Oleg L. Polyansky, Sergei N. Yurchenko, Jonathan Tennyson[1]

Department of Physics and Astronomy, University College London, London, WC1E 6BT, UK

Abstract

A room temperature line list for hydrogen peroxide is computed using on a high level *ab initio* potential energy surface by Małyszek and Koput [*J. Comput. Chem.* **34**, 337] with the small adjustment of the equilibrium geometry and height of the torsional barrier and a new *ab initio* dipole moment surface (CCSD(T)-f12b/aug-cc-pv(T+d)Z). In order to improve further the *ab initio* accuracy, the vibrational band centers were shifted to match experimental values when available. The line list covers the wavenumber region up to 8000 cm^{-1} with the rotational excitations $J \leq 40$. Room temperatures synthetic spectra of H_2O_2 are generated and compared to the spectra from the HITRAN and PNNL-IR databases showing good agrement.

Key words: Hydrogen peroxidr, dipole moment, infrared, transition dipole, vibration, HOOH, intensity, variational calculations

[1]Corresponding author

Email address: j.tennyson@ucl.ac.uk (Jonathan Tennyson)

1. Introduction

Hydrogen peroxide is trace species in Earth [1–3] atmospheric chemistry and plays a role in stratospheric ozone production. There have been multiple detections in the Martian [4–7] atmosphere, possibly formed by triboelectricity in dust devils and dust storms [6] and may well act as an agent in the oxidization of the Martian surface. A recent detection in the interstellar medium [8] gives insight to the formation of water in space. Finally it has been detected in the atmosphere of Europa [9] in the 3.5 μm ($\approx$2587.1 cm^{-1}) region.

Hydrogen peroxide is an asymmetric prolate motor molecule. Its most interesting characteristic is that it is the simplest molecule that exhibits internal (torsional) rotation. This gives it a double-minimum in its torsional potential as well as two alignments of the O-H bonds: *cis* and *trans*. The torsional mode therefore contains four 'sub-levels' for each excitation and requires an additional internal-rotation quantum number ($\tau = 1, 2, 3, 4$) [10] to properly chracterise it. It also only exhibits c-type transitions which consquently means it has no pure rotational transitions.

The HITRAN 2012 database [11] only contains transitions for hydrogen peroxide below 1800 cm^{-1}. This region covers the torsional, O-H bending modes and O-O stretch but misses the O-H stretches at the 3750 cm^{-1} region. Only a few studies deal with spectra of H_2O_2 in the mid-infrared and near-infrared [12–14] regions. Available rovibrational states mostly concern the torsional at ground and excited states [15] and the ν_3 [16] and ν_6 [14] vibrational modes. Whilst there is ample data available in the literature for the torsional and bending bands, the fundamental stretching modes are more difficult to obtain accurate term values for. The O-H stretching modes, v_1 and v_5, in particular have been especially problematic. The difference between the two bands are $\approx$ 8-10 cm^{-1} and torsional splitting from the double minimum of the potential gives rise to

doubling [17] in the form of 'quasi'-degenerate states [18] that are difficult to resolve with a degree of accuracy. Olsen et. al. [15] give an estimate of 3610 - 3618 cm^{-1} for ν_5 and 3601 - 3617 cm^{-1} for ν_1 whilst a Raman study gives a lower value of 3607 cm^{-1} [17] for the ν_1 band-center but determining the accuracy to better than 0.1 cm^{-1} is difficult. A theoretical line-list may provide a way of characterizing the confusing spectra of H_2O_2 above 1800 cm^{-1} but so far none have been produced.

In this work we present a room temperature line list based on the high quality *ab initio* potential energy [19, 20] and new dipole moment surfaces generated using the variational approach TROVE [21].

1.1. Method

The accuracy of the line positions is determined by the quality of the PES. The PES is based of the high-accuracy *ab initio* calculations of Małyszek and Koput Małyszekk and Koput [19] with the small adjustment of the *ab initio* equilibrium geometry and height of the torsional barrier proposed by Polyansky *et al* [20] who showed that boasting a root-mean-squares (rms) difference of 0.02 cm^{-1} for rotational levels up to $J = 35$ within low-lying vibrational states.

The rovibrational energies was calculated using the TROVE [21] computer suite. TROVE is a variational nuclear-motion solver and can be employed in all steps of line-list production for molecules of arbitrary structure. It has been successful to produce hot line lists for CH_4 [22], PH_3 [23], H_2CO [24] and room temperature ones for PH_3 [25] and SO_3 [26]. TROVE was also to simulate a room temperature spectrum for another non-rigid, chain molecule HSOH based on a high level *ab initio* potential energy and dipole moment surfaces [27] [28].

Within TROVE, the nuclear-motion Hamiltonian is represented as an expansion around a reference configuration where the bond lengths for the O-O bond (R), the O-H_1 bond (r_1) and the O-H_2 bond (r_2) and the bond angles for O-H_1

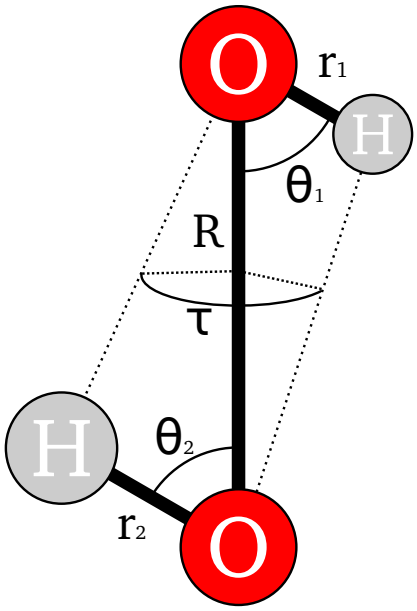

Figure 1: The internal co-ordinates of HOOH.

(θ_1) and O-H_2 (θ_2) are frozen at their equilibrium and the torsional angle τ varies on a grid of 10,000 values ranging from 0° to 720°. The internal co-ordinates are described in 1.

The kinetic energy is expanded around the reference geometry in terms of five linearized co-ordinates of the form:

$$\zeta_i = x_i^l - x_i^e \tag{1}$$

Where x_i^l and x_i^e represents linearized version and equilibrium geometry of the bond lengths and angles respectively. Here, $i = 1$, $i = 2$, $i = 3$, $i = 4$ and $i = 5$ represent R, r_1, r_2, θ_1 and θ_2 respectively and $i = 6$ is the sixth co-ordinate, $\zeta_6 = \tau$. Similarly the potential is expanded but the stretches are represented in terms of Morse-type functions for ζ_1,ζ_2 and ζ_3 and bending functions for ζ_4 and ζ_5. For this work the kinetic energy expansion order is 6 and the potential expansion order is 8.

A symmetry-adapted basis-set is constructed by a multi-step contraction

scheme that is truncated via polyad number $P_{\max} = 42$ [20]. The primitive vibrational basis-set is constructed by solving the 1D Schrodinger equation for each basis-function $\phi_{v_i}(\zeta_i)(i = 1, 2, ..., 6)$ associated with the vibrational quantum number v_i via Numerov-Cooley method [29, 30] for each mode allowed by the polyad P:

$$P = 4v_1 + 8(v_2 + v_3 + v_4 + v_5) + v_6 \leq P_{\max}. \tag{2}$$

The six dimensional co-ordinate space is then divided into four reduced subspaces: (ζ_1), (ζ_2, ζ_3), (ζ_4, ζ_5) and (ζ_6) based on symmetry. The reduced Hamiltonian is solved using the primitives ϕ_{v_i} as basis-functions to obtain the contracted vibrational basis-functions $\Phi_1(\zeta_1)$, $\Phi_2(\zeta_2, \zeta_3)$, $\Phi_3(\zeta_4, \zeta_5)$ and $\Phi_4(\zeta_6)$. These basis-functions are then symmetrised according to $\mathcal{D}_{2\mathrm{h}}$ symmetry and the final vibrational basis-set is formed from the product of the four contracted basis-functions which are truncated via Eq. (2) and symmetrized again. The general form of the Hamiltonian operator is:

$$H = H_{vib} + \frac{1}{2}\sum_{\alpha\beta} J_\alpha G_{\alpha\beta} J_\beta + \frac{1}{2}\sum_{\alpha\lambda}(p_\lambda G_{\lambda\alpha} + G_{\alpha\lambda} p_\lambda) J_\alpha, \tag{3}$$

where J_α and p_λ are the rotational and vibrational momentum operators repectively and H_{vib} is the pure vibrational ($J = 0$) Hamiltonian given as:

$$H_{vib} = \frac{1}{2}\sum_{\lambda\mu} p_\lambda G_{\lambda\mu} p_\mu + V + U, \tag{4}$$

where $G_{\alpha\beta}$ are kinetic energy factors, U is a pseudo-potential [21] and V is the molecular potential energy. The contracted Hamiltonian is solved up to an energy eigenvalue threshold of 24 000 cm^{-1}. A final contraction step can be performed by solving the $J = 0$ problem given by Eq. (4) and replacing the bulky primitive vibrational basis-sets with the more compact $J = 0$ wavefunctions. This has the added benefit of making the computation of the hamiltonian matrix elements for

$J > 0$ more efficient as the H_{vib} contribution becomes:

$$\langle \Psi^{\Gamma}_{J=0,i} | H_{vib} | \Psi^{\Gamma}_{J=0,i'} \rangle = E_{i,i'} \delta_{i,i'} \tag{5}$$

Where $\Psi^{\Gamma}_{J=0,i}$ is the symmetrized wavefunction of a particular state i obtained from Eq. (4). The vibrational contribution is both diagonal and simply the eigenvalue of $\Psi^{\Gamma}_{J=0,i}$. Additionally, experimental band centers can be substituted instead of the eigenvalues, this 'shifts' the band center onto the experimental value and allows further rotational excitations to be computed around the experimental band centers. Here the $J = 0$ wavefunctions with eigenvalues up to 8000 cm^{-1} are utilized further reducing the size of the hamiltonian. The original primitive basis-set was of size 2 789 400, this was reduced to 23 078 in the contracted and finally to 2875 using the $J = 0$ 'form'. A more detailed explanation of this methodology is given by Yurchenko et. al. [31].

Using these symmterized wavefunctions also has the benefit of the hamiltonian matrix being factorized into independant blocks according to $\mathcal{D}_{2h}$ symmetry. The $\mathcal{D}_{2h}$ is isomorphic to the $C^{+}_{2h}(M)$ symmetry group which best describes the torsional splitting caused by the *cis* and *trans* tunneling [32]. The irreducible representations of this group are A_g, A_u, B_{1g}, B_{1u}, B_{2g}, B_{2u}, B_{3g} and B_{3u}. However, the states corresponding to B_{2g}, B_{2u}, B_{3g} and B_{3u} have zero statistical weight and therefore their matrix blocks are not constructed and diagonalized for $J > 0$. It is usual to describe the H_2O_2 torsional modes using the notation (n, τ), where n describe the excitation of the torsional mode. The excitations of the torsional (υ_4/n) mode are representated by A_g, A_u, B_{2g} or B_{2u} symmetry which correspond to the quanta $\tau = 1$,$\tau = 4$,$\tau = 2$ and $\tau = 3$ respectively. This needs to be taken into account when manipulating the band-centers as it requires modifying the B_{2g} or B_{2u} eigenvalues in order to properly represent the splitting. Table 1 lists all the band-centers that were utilized in the empirical shifts together with the *ab initio* values before the shift.

The τ quantum number can be preserved in the quantum number assignment in TROVE by utilizing the following form:

$$v_4 = 4n + i, \tag{6}$$

where n is the excitation and i is the symmetry where $i = 0, 1, 2, 3$ is A_g, B_{2g}, B_{2u} and A_u respectively. To retrieve n and τ is simply:

$$\tau = (v_4 \bmod 4) + 1, \quad n = \frac{v_4}{4} \tag{7}$$

The final line-list format will extract both numbers and utilize n as the value for v_4 and include a separate τ quantum number which should not be confused with the commonly used rotational parity symbol $\tau_{\text{rot}} = \pm$ or with the torstional angle τ (see bellow). Towards this line-list, the Hamiltonian matrices up to the limit of $J = 40$ are constructed and diagonalized using the $J = 0$ contracted basis set for all eigenvalues and eigenvectors but only eigenvectors up to 8000 $cm^{-1}$are stored and used in producing the transitions.

1.2. Dipole moment surface and intensities

An electric dipole moment surface (DMS) is required to compute the absolute intensities for each transition. An *ab initio* DMS computed at the CCSD(T)-f12b/aug-cc-pV(T+d)Z [35] level of theory in the frozen-core approximation using CCSD(T) [36] on a grid of 50 000 geometries in conjunction with the finite electric field method and field of 0.005 a.u.. The $\mathcal{D}_{2h}$ symmetry-adapted projections of the dipole moment Cartesian components μ_x, μ_y, and μ_z are given in the analytical representations with each component expanded in Taylor series (312 parameters in total) in terms of internal coordinates around the equilibrium configuration using a molecular-fixed axis system as follows. The z axis is aligned along the O-O bond, and the x axis lies in the plane bisecting the two O-O-H planes (i.e. planes containing the O-O and O-H bonds). The y axis is oriented such that

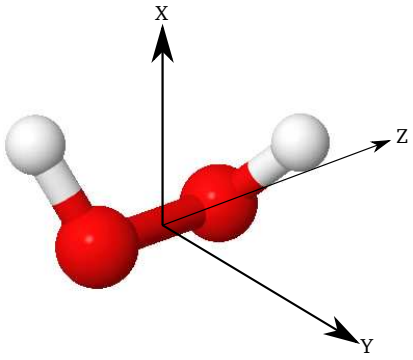

Figure 2: The principal axis for HOOH used in the DMS expansion.

the xyz axis system is right-handed. This xyz axes is not exactly but close to the principal axis system shown in 2 With the chosen axes, the x, y, and z components of the dipole moment span the B_{1u}, B_{3u}, and B_{2u} representations, respectively. The three electronically averaged dipole components are represented by the following analytical functions:

$$\bar{\mu}_x = \cos(\tau/2) \sum_{i_1,i_2,\ldots,i_6} \mu^{(x)}_{i_1,i_2,\ldots,i_6} \xi_1^{i_1} \xi_2^{i_2} \xi_3^{i_3} \xi_4^{i_4} \xi_5^{i_5} \xi_6^{i_6}, \tag{8}$$

$$\bar{\mu}_y = \sin(\tau/2) \sum_{i_1,i_2,\ldots,i_6} \mu^{(y)}_{i_1,i_2,\ldots,i_6} \xi_1^{i_1} \xi_2^{i_2} \xi_3^{i_3} \xi_4^{i_4} \xi_5^{i_5} \xi_6^{i_6}, \tag{9}$$

$$\bar{\mu}_z = \sum_{i_1,i_2,\ldots,i_6} \mu^{(z)}_{i_1,i_2,\ldots,i_6} \xi_1^{i_1} \xi_2^{i_2} \xi_3^{i_3} \xi_4^{i_4} \xi_5^{i_5} \xi_6^{i_6}, \tag{10}$$

where

$$\xi_1 = \Delta R e^{-(\Delta R)^2}, \tag{11}$$

$$\xi_2 = \Delta r_1 e^{-(\Delta r)^2}, \tag{12}$$

$$\xi_3 = \Delta r_2 e^{-(\Delta r)^2}, \tag{13}$$

$$\xi_4 = \Delta\theta_1, \tag{14}$$

$$\xi_5 = \Delta\theta_2, \tag{15}$$

$$\xi_6 = \cos\tau. \tag{16}$$

$$\tag{17}$$

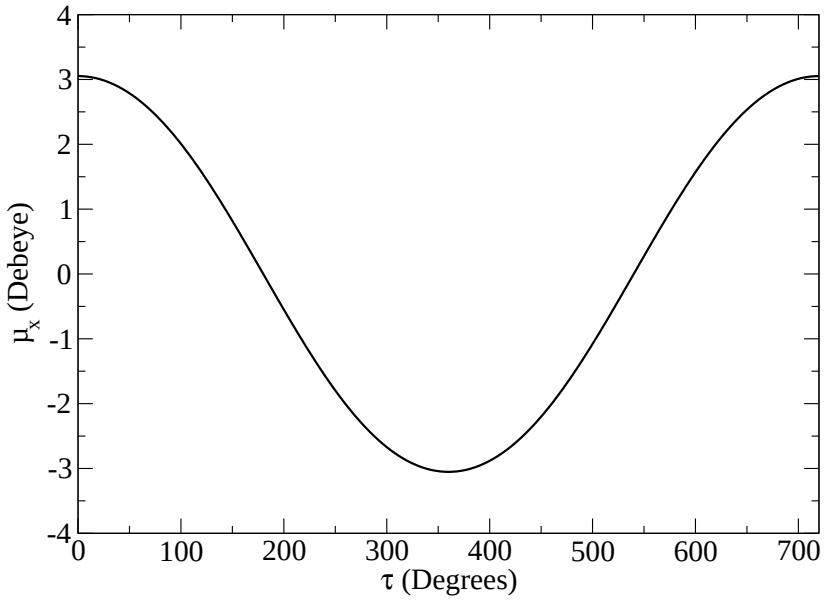

Figure 3: The μ_x dipole moment component for H_2O_2, computed at the torsional geometries shown

The expansion parameters of the y and z components of the dipole obey the following permutation rule:

$$\mu^{(\alpha)}_{i_1,i_2,i_3,i_4,i_5,i_6} = -\mu^{(\alpha)}_{i_1,i_3,i_2,i_5,i_4,i_6} \tag{18}$$

corresponding to the permutation of the two hydrogen atoms and therefore $\mu^{(\alpha)}_{0,0,0,0,0,i_6} = 0$ ($\alpha = y, z$) for any i_6. The dependance of μ_x component against the torsional angle is shown in 3.

The 130, 90, and 92 symmetrically independent expansion parameters $\mu^{(\alpha)}_{i_1,i_2,i_3,i_4,i_5,i_6}$ ($\alpha = x, y, z$) were obtained in a least-squares fit to the $3 \times 20\,842$ *ab initio* dipole moment values (corresponding to energies below $hc12\,000$ cm^{-1}) with the rms error of 0.0013, 0.0002, and 0.0010 D, respectively. The resulting DMS parameters are given in the supplementary material.

In TROVE the *ab initio* DMS is re-expanded around the non-rigid reference configuration in terms of the ζ_i ($i = 1 \ldots 5$) variables as described above, using

the numerical finite differences method [21]. At some torsional values close to $\tau = 360°$ and $\tau = 720°$ the finite differences produce discontinuities, which lead to meaningless values of the dipole expansion parameters $\mu_{i,j,k}(\tau)$ for a number of grid points. These points are treated as outliers and replaced by interpolated values. Additionally as the expansion is not an exact representation of the τ_x dipole component it may display artifical asymmetry. This is resolved by computing τ_x for torsional geometries up to $\tau = 360°$ and then mirroring the values up to $\tau = 720°$

The vibrational transition moment is computed as such:

$$\mu_{if} = \sqrt{\sum_{A=x,y,z} |\langle \Psi^{\Gamma}_{J=0,i} | \bar{\mu}_A | \Psi^{\Gamma}_{J=0,f} \rangle|^2} \tag{19}$$

Our vibrational transition moment for the ground vibrational state 1.5683 D and compares well with measured of 1.5728 D [37]. This is very different from the equilibrium value of the *ab initio* dipole moment $\bar{\mu}^{\mathrm{e}}_x = 1.738$ D (at $R = 1.4554$ Å, $r_1 = r_2 = 0.96257$ Å, $\theta_1 = \theta_2 = 101.083°$), showing strong non-rigid character of the H_2O_2 dipole moment.

Information on transition moments for H_2O_2 is limited; 2 compares available experimentally derived values at different torsional excitations from experiment [13]. Our calculated values reproduce the experimental with a maximum deviation of 2.4%. Some papers report effective transition dipole moments as a torsional expansion in terms of τ, e.g. $\cos \tau\phi_z$ [13] which are difficult to compare to our fully averaged transition dipoles.

Using the DMS and eigenvectors obtained from diagonalization, the linestrengths for each transition can be computed providing they satify the selection rules:

$$J' - J'' = 0, \pm 1, J' + J'' \neq 0 \tag{20}$$

and

$$A_g \leftrightarrow A_u \ , B_{1g} \leftrightarrow B_{1u} \tag{21}$$

and the B_{2g}, B_{2u}, B_{3g} and B_{3u} are forbidden duo the the nuclear statistics. The Einstein-A coefficient for a particular transition from the *initial* state i to the *final* state f is given by:

$$A_{if} = \frac{8\pi^4 \tilde{\nu}_{if}^3}{3h}(2J_i + 1) \sum_{A=X,Y,Z} |\langle \Psi^f | \bar{\mu}_A | \Psi^i \rangle|^2, \tag{22}$$

where J_i is the rotational quantum number for the initial state, h is Planck's constant, $\tilde{\nu}_{if}$ is the transition frequency ($hc\,\tilde{\nu}_{if} = E_f - E_i$), Ψ^f and Ψ^i represent the eigenfunctions of the final and initial states respectively, $\bar{\mu}_A$ is the electronically averaged component of the dipole moment along the space-fixed axis $A = X, Y, Z$ (see also Yurchenko et al. [38]). From this the absolute absorption intensity is determined by:

$$I(f \leftarrow i) = \frac{A_{if}}{8\pi c} g_{\rm ns}(2J_f + 1) \frac{\exp\left(-\frac{E_i}{kT}\right)}{Q\ \tilde{\nu}_{if}^2} \left[1 - \exp\left(\frac{-hc\tilde{\nu}_{if}}{kT}\right)\right], \tag{23}$$

where k is the Boltzmann constant, T the absolute temperature and $g_{\rm ns}$ is the nuclear spin statistical weight factor. Q, the partition function, is given by:

$$Q = \sum_i g_i \exp\left(\frac{-E_i}{kT}\right), \tag{24}$$

where g_i is the degeneracy of a particular state i with energy E_i. For H_2O_2, g_i is $g_{\rm ns}(2J_i + 1)$ with $g_{\rm ns} = 1$ for A_g and A_u, $g_{\rm ns} = 3$ for B_{1g} and B_{1u} and $g_{\rm ns} = 0$ for the B_{2g}, B_{2u}, B_{3g} and B_{3u} symmetries. The transitions were computed using the energy limits hc 4 000 and hc 8 000 cm^{-1} for the lower and upper states, respectively to acheive our target $\tilde{\nu}_{if}$ limit of 8 000 cm^{-1}. The recently developed GAIN (GPU Accelerated INtensities) code was utilized to compute 1 487 073 009 transitions within 6 hours by exploiting M2090 nVidia graphics processing units (GPU) for their high degree of parallelism and computational efficiency. A paper discussing the methodolgy in detail will be published elsewhere [39].

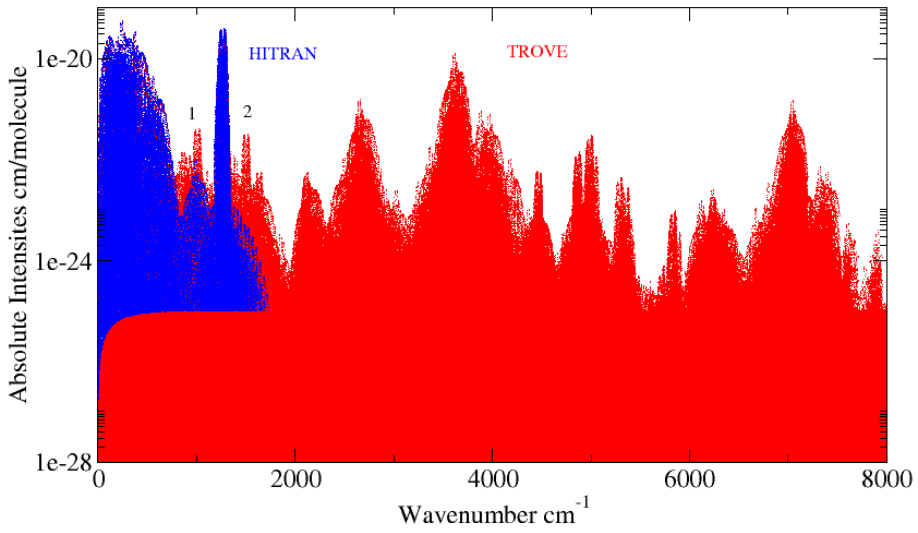

Figure 4: Overview of our synthetic spectrum at T =296 K against HITRAN [11]

2. Results

Using our line-list we obtained the partition function of 9840.91 which compares well to the HITRAN value 9819.80 [40].

Figure 4 is our synthetic spectrum at 296 K for all 1.4 billion lines and comparing against the 126,983 lines from HITRAN highlights the significant degree of completeness our line-list provides. However two regions (1) and (2) show disagreement in line intensity, which can be attributed to the lack of the experimental data used for producing the HITRAN intensities by Perrin et. al [13, 14].

The PNNL-IR [41] database provides additional cross-sections above 1800 cm^{-1}. Figure 5 compares ours and HITRAN's simulated cross-sections to PNNL using a Gaussian convolution with HWHM at 0.312 cm^{-1} at T=323.15 K and demonstrates that we agree mich better in intensity and structure indicating problems with HITRAN intensities for both of the two regions.

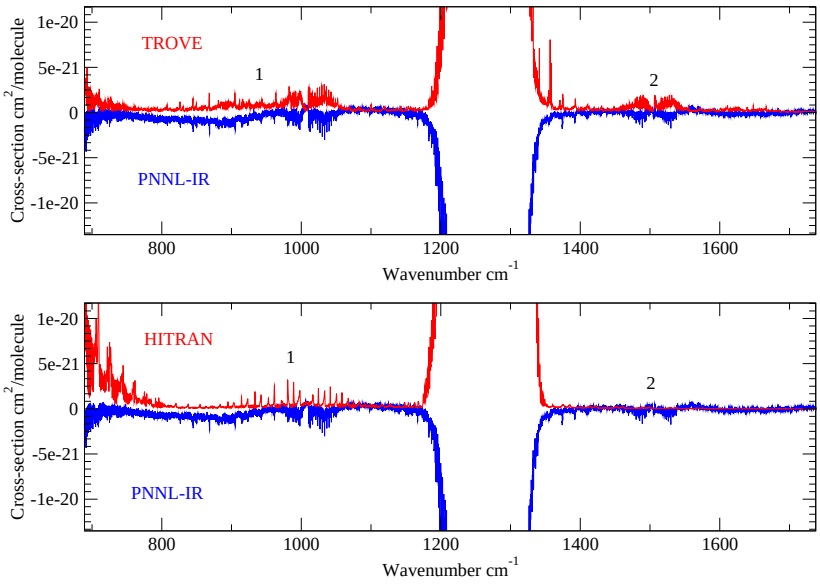

Figure 5: Cross-section comparison of the room temperature line-list against experimental PNNL-IR [41] data at the v_1 and v_5 band at 323.15 K with HWHM = 0.3120 cm^{-1}.

Figure 6 highlights a band in the 3.5 μm region which is a combination of the $(0, \tau = 1) \rightarrow (\nu_3 + 6\nu_4, \tau = 1)$, $(0, \tau = 1) \rightarrow (2\nu_3 + 4\nu_4, \tau = 1)$, $(0, \tau = 2) \rightarrow (3\nu_3, \tau = 1)$, $(0, \tau = 2) \rightarrow (\nu_3 + \nu_4 + \nu_5, \tau = 2)$, $(0, \tau = 3) \rightarrow (\nu_3 + 4\nu_4, \tau = 4)$ and other weaker hot bands. Good agreement is seen in both structure and overall intensity but our 'guessed' line profile utilized in our convolution may not be adequate enough to properly replicate the PNNL-IR cross-section leading to some minor differences in the overall cross-section.

Figure 7 further states the quality of both the line-positions and absolute intensities by comparing the ν_1 and ν_5 (ours vs PNNL-IR's) bands in the 2.7 μm region. As this is the region of most contention in the literature, it is hopeful that this line-list may provide a means with which to identify the confusing spectra in this region

Finally, the importance of the band shift previously discussed is illustrated in 8. Here the TROVE-I spectra is purely using the *ab initio* band centers

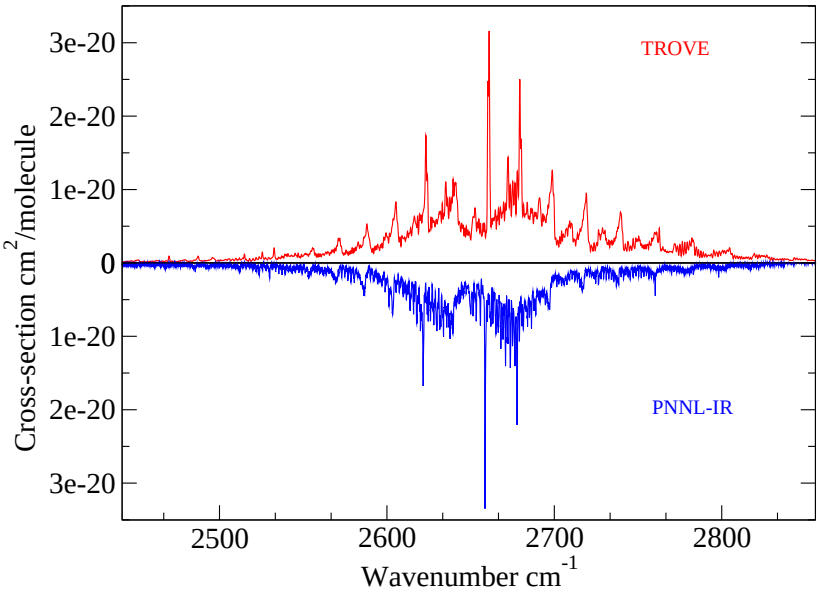

Figure 6: Cross-section comparison of the room temperature line-list against experimental PNNL-I

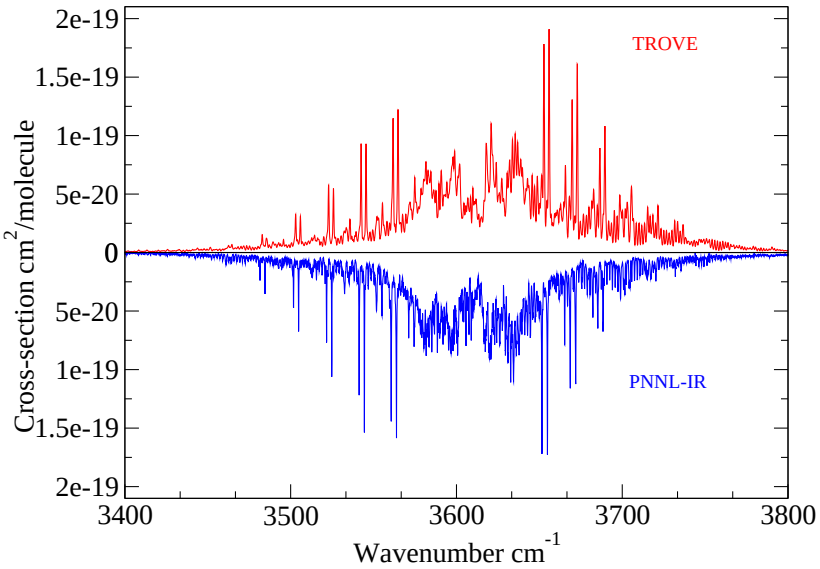

Figure 7: Cross-section comparison of the room temperature line-list against experimental PNNL-IR [41] data at the ν_1 and ν_5 band at 323.15 K with HWHM = 0.3120 cm^{-1}.

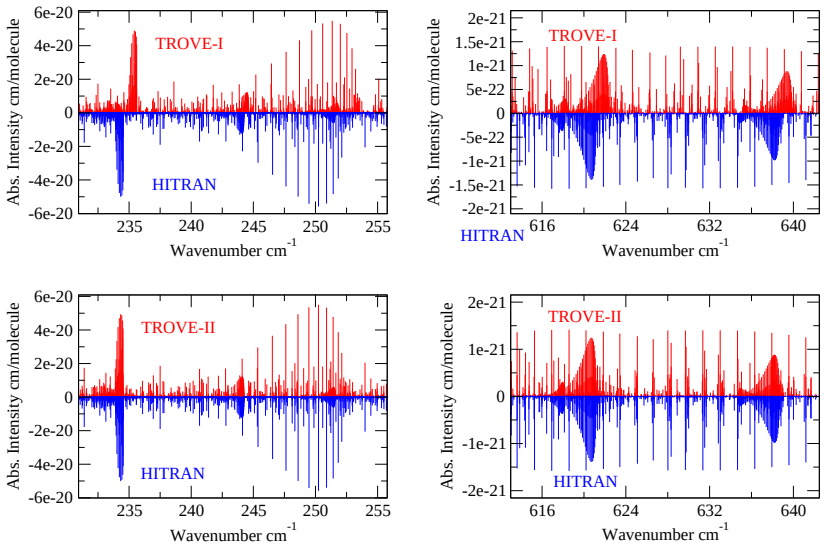

Figure 8: Comparing two versions of the synthetic spectrum against HITRAN at T=295 K. TROVE-I is the *ab initio*, TROVE-II is using the empirical band-center shifts.

while TROVE-II utilizes the experimental band centers from 1. The *ab initio* deviation of 1.12 cm^{-1} reduces significantly to 0.005 cm^{-1} using this empirical shifting method.

3. Conclusions

Presented here is a high-quality room temperature line-list for H_2O_2 that covers the region up to 8000 cm^{-1}. The complete line-list is available at Exomol website: http://www.exomol.com. The ultimate goal is for a hot line-list for H_2O_2 that reaches up to 10 000 cm^{-1}. Whilst there is extremely good agreement in both line-positions and intensities, the current strategy is to refine the PES into a new semi-empirical PES. The band-center shifting does resolve many discrepancies between the theoretical and experimental energy, however, due to the lack of line-positions, it may be not as accurate in predicting the nature of the ν_1 and ν_5 bands. By applying the refinement process, it may bring the PES closer

to the 'true' form giving better predictions in this troublesome region. Nevertheless, this line-list can produce synthetic spectra that agree well with room temperature.

Acknowledgments

This work was supported by the ERC under the Advanced Investigator Project 267219 and made use of the DiRAC@Darwin, DiRAC@COSMOS HPC cluster and Emerald CfI cluster. DiRAC is the UK HPC facility for particle physics, astrophysics and cosmology and is supported by STFC and BIS. The authors would like to acknowledge the work presented here made use of the EMERALD High Performance Computing facility provided via the Centre for Innovation (CfI). The CfI is formed from the universities of Bristol, Oxford, Southampton and UCL in partnership with STFC Rutherford Appleton Laboratory. RIO thanks the Russian Fund for Fundamental Studies, Project 15-02-07887 A. AFA would also like to thank Dr. Faris N. Al-Refaie, Lamya Ali, Sarfraz Ahmed Aziz and Rory and Annie Gleeson for their support.

References

[1] D. D. Davis, Can. J. Chem. 52 (1974) 1405–1414.

[2] N. D. C. Allen, G. G. Abad, P. F. Bernath, C. D. Boone, J. Quant. Spectrosc. Radiat. Transf. 115 (2013) 66–77.

[3] K. V. Chance, D. G. Johnson, W. A. Traub, K. W. Jucks, Geophys. Res. Lett. 18 (1991) 1003–1006.

[4] S. Aoki, M. Giuranna, Y. Kasaba, H. Nakagawa, G. Sindoni, A. Geminale, V. Formisano, Icarus 245 (2015) 177–183.

[5] T. Encrenaz, B. Bezard, T. K. Greathouse, M. J. Richter, J. H. Lacy, S. K. Atreya, A. S. Wong, S. Lebonnois, F. Lefevre, F. Forget, Icarus 170 (2004) 424–429.

[6] T. Encrenaz, T. K. Greathouse, F. Lefevre, S. K. Atreya, Planet Space Sci. 68 (2012) 3–17.

[7] R. T. Clancy, B. J. Sandor, G. H. Moriarty-Schieven, Icarus 168 (2004) 116–121.

[8] P. Bergman, B. Parise, R. Liseau, B. Larsson, H. Olofsson, K. M. Menten, R. Güsten, Astron. Astrophys. 531 (2011) L8.

[9] K. P. Hand, M. E. Brown, Astrophys. J. Lett. 766 (2013) L21.

[10] R. H. Hunt, R. A. Leacock, C. W. Peters, K. T. Hecht, J. Chem. Phys. 42 (1965) 1931–1946.

[11] L. S. Rothman, I. E. Gordon, Y. Babikov, A. Barbe, D. C. Benner, P. F. Bernath, M. Birk, L. Bizzocchi, V. Boudon, L. R. Brown, A. Campargue, K. Chance, E. A. Cohen, L. H. Coudert, V. M. Devi, B. J. Drouin, A. Fayt, J.-M. Flaud, R. R. Gamache, J. J. Harrison, J.-M. Hartmann, C. Hill, J. T. Hodges, D. Jacquemart, A. Jolly, J. Lamouroux, R. J. Le Roy, G. Li, D. A. Long, O. M. Lyulin, C. J. Mackie, S. T. Massie, S. Mikhailenko, H. S. P. Müller, O. V. Naumenko, A. V. Nikitin, J. Orphal, V. Perevalov, A. Perrin, E. R. Polovtseva, C. Richard, M. A. H. Smith, E. Starikova, K. Sung, S. Tashkun, J. Tennyson, G. C. Toon, V. G. Tyuterev, G. Wagner, J. Quant. Spectrosc. Radiat. Transf. 130 (2013) 4 – 50.

[12] L. A. Zumwalt, P. A. Giguere, J. Chem. Phys. 9 (1941) 458–462.

[13] A. Perrin, J.-M. Flaud, C. CamyPeyret, R. Schermaul, M. Winnewisser, J.-Y. Mandin, V. Dana, M. Badaoui, J. Koput, J. Mol. Spectrosc. 176 (1996) 287–296.

[14] A. Perrin, A. Valentin, J. M. Flaud, C. Camy-Peyret, L. Schriver, A. Schriver, P. Arcas, J. Mol. Spectrosc. 171 (1995) 358–373.

[15] W. B. Olson, R. H. Hunt, B. W. Young, A. G. Maki, J. W. Brault, J. Mol. Spectrosc. 127 (1988) 12–34.

[16] C. Camy-Peyret, J.-M. Flaud, J. W. C. Johns, M. Noel, J. Mol. Spectrosc. 155 (1992) 84–104.

[17] P. A. Giguere, T. K. K. Srinivasan, Journal of Raman Spectroscopy 2 (1974) 125–132.

[18] G. Rauhut, G. Knizia, H.-J. Werner, J. Chem. Phys. 130 (2009) 054105.

[19] P. Małyszekk, J. Koput, J. Comput. Chem. 34 (2013) 337–345.

[20] O. L. Polyansky, I. N. Kozin, P. Maĺyszek, J. Koput, J. Tennyson, S. N. Yurchenko, J. Phys. Chem. A 117 (2013) 7367–7377.

[21] S. N. Yurchenko, W. Thiel, P. Jensen, J. Mol. Spectrosc. 245 (2007) 126–140.

[22] S. N. Yurchenko, J. Tennyson, Mon. Not. R. Astron. Soc. 440 (2014) 1649–1661.

[23] C. Sousa-Silva, A. F. Al-Refaie, J. Tennyson, S. N. Yurchenko, Mon. Not. R. Astron. Soc. 446 (2015) 2337–2347.

[24] A. F. Al-Refaie, S. N. Yurchenko, A. Yachmenev, J. Tennyson, Mon. Not. R. Astron. Soc. 448 (2015) 1704–1714.

[25] C. Sousa-Silva, S. N. Yurchenko, J. Tennyson, J. Mol. Spectrosc. 288 (2013) 28–37.

[26] D. S. Underwood, J. Tennyson, S. N. Yurchenko, Phys. Chem. Chem. Phys. 15 (2013) 10118–10125.

[27] S. N. Yurchenko, A. Yachmenev, W. Thiel, O. Baum, T. F. Giesen, V. V. Melnikov, P. Jensen, J. Mol. Spectrosc. 257 (2009) 57–65.

[28] A. Yachmenev, S. N. Yurchenko, P. Jensen, O. Baum, T. F. Giesen, W. Thiel, Phys. Chem. Chem. Phys. 12 (2010) 8387–8397.

[29] B. V. Noumerov, Mon. Not. R. Astron. Soc. 84 (1924) 592–602.

[30] J. W. Cooley, Math. Comp. 15 (1961) 363–374.

[31] S. N. Yurchenko, R. J. Barber, A. Yachmenev, W. Thiel, P. Jensen, J. Tennyson, J. Phys. Chem. A 113 (2009) 11845–11855.

[32] J. T. Hougen, Can. J. Phys. 62 (1984) 1392–1402.

[33] J.-M. Flaud, C. Camy-Peyret, J. W. C. Johns, B. Carli, J. Chem. Phys. 91 (1989) 1504–1510.

[34] A. Perrin, J.-M. Flaud, C. Camy-Peyret, A. Goldman, F. J. Murcray, R. D. Blatherwick, J. Mol. Spectrosc. 142 (1990) 129–147.

[35] R. J. Bartlett, M. Musiał, Rev. Mod. Phys. 79 (2007) 291–352.

[36] H.-J. Werner, P. J. Knowles, G. Knizia, F. R. Manby, M. Schütz, WIREs Comput. Mol. Sci. 2 (2012) 242–253.

[37] E. Cohen, H. Pickett, J. Mol. Spectrosc. 87 (1981) 582 – 583.

[38] S. N. Yurchenko, W. Thiel, M. Carvajal, H. Lin, P. Jensen, Adv. Quant. Chem. 48 (2005) 209–238.

[39] A. F. Al-Refaie, J. Tennyson, S. N. Yurchenko, Comput. Phys. Commun. (2015). (to be submitted).

[40] J. Fischer, R. R. Gamache, A. Goldman, L. S. Rothman, A. Perrin, J. Quant. Spectrosc. Radiat. Transf. 82 (2003) 401–412.

[41] S. W. Sharpe, T. J. Johnson, R. L. Sams, P. M. Chu, G. C. Rhoderick, P. A. Johnson, Appl. Spectrosc. 58 (2004) 1452–1461.

Table 1: Experimental [15, 16, 33, 34] band centers used in the empirical shift.

v_1	v_2	v_3	n	v_5	v_6	τ	Symmetry	Ab-Initio (cm^{-1})	Shifted/Obs (cm^{-1})
0	0	0	0	0	0	4	A_u	11.312	11.437
0	0	0	0	0	0	3	B_{2u}	11.312	11.437
0	0	0	1	0	0	1	A_g	255.529	254.55
0	0	0	1	0	0	2	B_{2g}	255.532	254.55
0	0	0	1	0	0	4	A_u	371.589	370.893
0	0	0	1	0	0	3	B_{2u}	371.590	370.893
0	0	0	2	0	0	1	A_g	570.809	569.743
0	0	0	2	0	0	2	B_{2g}	570.818	569.743
0	0	0	2	0	0	4	A_u	777.432	776.1221
0	0	0	2	0	0	3	B_{2u}	777.458	776.1148
0	0	1	0	0	0	1	A_g	865.539	865.939
0	0	1	0	0	0	2	B_{2g}	865.539	865.939
0	0	1	0	0	0	4	A_u	877.470	877.934
0	0	1	0	0	0	3	B_{2u}	877.470	877.934
0	0	0	3	0	0	1	A_g	1002.666	1000.882
0	0	0	3	0	0	2	B_{2g}	1002.869	1000.93
0	0	0	0	0	1	1	B_{1u}	1265.003	1264.583
0	0	0	0	0	1	3	B_{1g}	1285.879	1285.121
0	0	0	1	0	1	1	B_{1u}	1506.164	1504.872
0	0	0	1	0	0	3	B_{1g}	1649.977	1648.367
0	0	0	2	0	1	1	B_{1u}	1855.823	1853.634
0	0	0	2	0	1	3	B_{1g}	2075.366	2072.404

Table 2: Absolute values of experimental [13] and *ab initio* transition moments, in debye, for $(n', \tau = 1) \leftrightarrow (n'', \tau = 3)$.

n'	n''	Calc	Obs	(Obs-Calc)/Obs (%)
0	0	1.5683	1.5723	0.25
0	1	0.3332	0.3413	-2.40
1	0	0.6031	0.6136	-1.72
1	1	1.1664	1.1751	0.74
2	1	1.1664	1.1628	0.31
2	2	1.2638	1.2825	1.46
3	2	1.3276	1.3535	-1.91